Reflectometry with Polarized Neutrons on In Situ Grown Thin Films

Wolfgang Kreuzpaintner, Andreas Schmehl, Alexander Book, Thomas Mairoser, Jingfan Ye, Birgit Wiedemann, Sina Mayr, Jean-François Moulin, Jochen Stahn, Dustin A. Gilbert, Henrik Gabold, Zahra Inanloo-Maranloo, Michael Heigl, Sergey Masalovich, Robert Georgii, Manfred Albrecht, Jochen Mannhart, and Peter Böni*

Originating from the demand for obtaining depth-resolved magnetization profiles from thin films and heterostructures, polarized neutron reflectometry (PNR) has developed into a unique research tool, which also finds application in the analysis of superconducting or soft matter thin films. While certain in situ sample environments such as gas-loading or humidity cells were quickly realized after PNR first emerged, preparing and growing thin magnetic films directly in the neutron beam could only be realized in recent years. Herein, a dedicated insight is given on the history and development of in situ thin film growth capabilities for PNR, from early pioneering experiments to the present day. The scientific and technological challenges as well as the advances of neutron sources, neutronics, and data treatment that have led to its realization are highlighted together with the unique research opportunities that it provides and recently obtained experimental results.

1. Introduction

Our understanding of materials would be only rudimentary if it was not for electromagnetic waves and subatomic particles that allow the secrets of nature to be discovered. Complementing the information gained by electron- and photon-based scattering techniques, neutrons are unique in their applications. Neutron scattering not only provides information on the distribution of elements or isotopes, but also enables the simultaneous retrieval of structural and magnetic properties on the atomic scale.

Thin magnetic layers constitute the basic modules from which many of today's electronic devices are composed. They are almost exclusively manufactured using sophisticated deposition techniques,

W. Kreuzpaintner
Institute of High Energy Physics
Chinese Academy of Sciences (CAS)
Beijing 100049, China/c

W. Kreuzpaintner
Spallation Neutron Source Science Center (SNSSC)
No. 1 Zhongziyuan Road, Dalang 523803, China/c

W. Kreuzpaintner, A. Book, J. Ye, B. Wiedemann, S. Mayr,[+] H. Gabold,
Z. Inanloo-Maranloo, P. Böni
Physik-Department E21
Technische Universität München
James-Franck-Str. 1, Garching 85748, Germany
E-mail: peter.boeni@frm2.tum.de/c

The ORCID identification number(s) for the author(s) of this article can be found under https://doi.org/10.1002/pssb.202100153.

[+]Present address: Paul Scherrer Institut (PSI), CH-5232 Villigen, Switzerland

A. Schmehl, T. Mairoser, M. Heigl, M. Albrecht
Institut für Physik
Universität Augsburg
Universitätsstraße 1, Augsburg 86159, Germany/c

J.-F. Moulin
German Engineering Materials Science Centre (GEMS)
Heinz Maier-Leibnitz Zentrum (MLZ)
Helmholtz-Zentrum Geesthacht GmbH
Lichtenbergstr. 1, Garching bei München 85747, Germany/c

J. Stahn
Laboratory for Neutron Scattering and Imaging
Paul Scherrer Institut (PSI)
Villigen CH-5232, Switzerland/c

D. A. Gilbert
Department of Materials Science and Engineering
University of Tennessee
Knoxville, TN 37996, USA/c

S. Masalovich, R. Georgii
Heinz Maier-Leibnitz Zentrum (MLZ, FRM II)
Technische Universität München
Lichtenbergstr. 1, Garching 85748, Germany/c

J. Mannhart
Solid State Quantum Electronics
Max-Planck-Institut für Festkörperforschung
Heisenbergstraße 1, 70 569 Stuttgart, Germany/c

including sputter deposition, pulsed laser deposition (PLD), and molecular beam epitaxy (MBE).

Thin films have become increasingly more sophisticated, with multiple functional layers, comprising a variety of elements, prepared with monolayer precision.[1–4] Leveraging the multilayer structure, fundamental properties, such as magnetic and electronic ordering, can be entangled. As a thin layer forms, its structure, the stoichiometry, and defect population evolve. These define functional properties of the film and thus the functionality of the final device. With increasing complexity of thin film devices, understanding the underlying physics has become increasingly challenging, but also increasingly critical.

From polarized neutron reflectometry (PNR) depth-resolved average nuclear and magnetic profiles can be obtained, which hold information on the interfaces and bulk structures of individual thin films. This information includes the number density and roughness, saturation magnetization and magnetic orientation, and even buried structures.[5–13] Characterizing thin film heterostructures with PNR during their growth would be a powerful analytical tool, which is in principle applicable to most vapor-based thin film growth techniques, including MBE, PLD, thermal laser evaporation (TLE),[14] and sputtering.

Progressive advances in neutron source brilliance[15] (**Figure 1**), neutron optics, and instrument design have collectively improved the signal and signal-to-noise ratio of neutron experiments to the point that such experiments have become practical. These new capabilities allow research to address how the microstructure, and if applicable, magnetic properties of heterostructures form, are correlated with each other, and how they evolve during growth.

1.1. Scientific Environment for In Situ PNR

The investigation of magnetic properties constitutes a central area of solid state physics research in which neutron scattering has proven to be an indispensable and powerful tool.
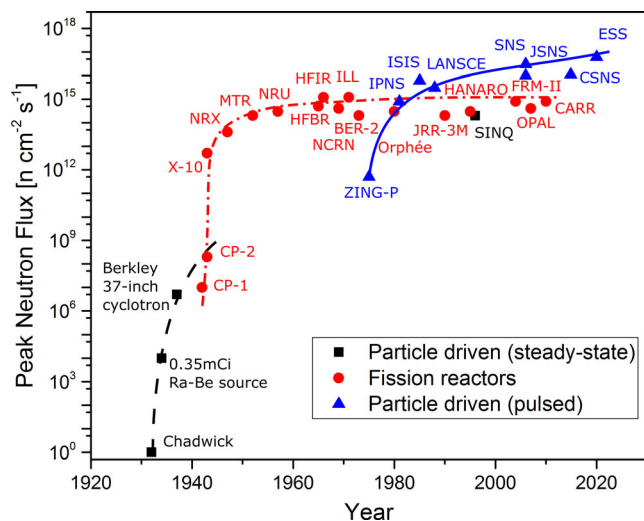

Figure 1. Evolution of the peak neutron flux of major neutron sources versus year of initial operation.

Thin film growth performed in situ with PNR measurements offers an opportunity to investigate emergent collective behavior, such as magnetism, ferroelectricity, and superconductivity in single-layer films or interactions between materials in hetereostructures.

The complexity, particularly in heterostructures, originates from an interplay of various effects, such as exchange coupling, uniaxial magnetic anisotropy, surface and interface magnetism, and localized conductance channels and pockets. Controlling these materials and interactions by external influences—such as magnetic or electric fields, temperature, or pressure—is generally aimed for. Some of the potential applications of in situ PNR, its advantages, and the present experimental realizations are outlined in the following.

1.1.1. Advantages of In Situ PNR

PNR gives simultaneously access to the structural and magnetic properties by a single analysis technique and is highly sensitive to even weak magnetic signals from buried layers or interfaces that are not accessible by conventional laboratory methods.

To elucidate trends with traditional ex situ PNR requires multiple, nominally identical samples to be prepared and measured, which may differ only in one aspect, such as the layer thickness or a thickness-dependent composition, or number of multilayers. In situ PNR allows a single sample to be used and systematically investigated without the need of any realignment or concerns of sample variation.

Beyond the systematic monitoring of the thin film growth, in situ techniques have many other advantages. For example, in situ PNR allows sensitive samples to be measured without a protective capping layer, which could alter the properties.[16,17] These systems have become increasingly common with topological materials, in which the surface is severely affected by neighboring layers.

The possibility to deposit a material onto an underlayer during or sequentially with a measurement process enables the study of dynamic processes such as topotactic transformation[18] and chemical reduction of oxides with metallic thin films.[19–22] The fact that the sample is directly grown at the neutron beamline also eliminates the time required for exchanging samples, which can be particularly burdensome if the samples are small, absorptive, or rough; this is especially true if the samples need to be cooled or heated to a measurement temperature. In addition, it also allows researchers to quickly respond to novel scientific results and actively adapt their research strategy.

A very important aspect to be noted is that in PNR the only measured quantity is the reflected intensities $I(q_z)$ to which theoretical models are fitted with the objective of deducting the scattering length density (SLD) profile that reproduces the measured reflectivity best. The fits take into account mainly four key parameters of the PNR curves: 1) the critical scattering vector up to which total reflection occurs, revealing the scattering length density of each layer, 2) the periodic Kiessig fringes, a measure of the layer thicknesses, 3) the decay of the reflectivity curves that exceeds the expected decrease in the Fresnel reflectivity, a measure for the interfacial root-mean-square (rms) roughness of interfaces, and 4) the spin dependence of the reflectivity. The non-spin–flip channels encode the in-plane magnetization

parallel and antiparallel to the neutron spin, whereas the spin–flip channels, with the incident and scattered neutrons having opposite orientations, encode the in-plane magnetization orthogonal to the neutron spin.

The converged SLD profiles are, however, not necessarily unique to a particular $I(q_z)$, as either symmetry-related[23] or even widely differing theoretical SLD profiles can result in indistinguishably identical "best fit" results. Here, in situ PNR provides a large a priori knowledge of a sample's history that allows nonphysical solutions to be identified and discarded during the fit process. By performing a series of measurements on a sample that is sequentially grown in situ, the uniqueness of the fits as a whole is increased. Ultimately, in situ PNR also represents a novel approach to analytical methods that apply direct inversion algorithms to obtain a unique solution of the sample structure (Section 3.4).

1.1.2. Existing Experimental Utilization of In Situ PNR

Although in situ characterization of thin films by electron- and photon-based probes[24,25] as well as by scanning probe techniques[26,27] is common practice, reports on PNR performed on in situ grown thin films are extremely rare in the literature. The earliest known PNR thin film experiments that had a deposition system in the neutron beam date back to August 1997, when, at the NIST Center for Neutron Research (NCNR), the dependence of the magnetic exchange coupling between Fe layers in Fe/V superlattices on the uptake of hydrogen by V was investigated.[28] The applied in situ MBE was designed specifically for the growth of high-quality thin films and immediate measurement without breaking vacuum. This system leveraged an aluminum chamber to allow neutron transmission, with the sample oriented vertically for a horizontal scattering plane. Up to four substrates could be preloaded into an auxiliary ultra-high vacuum (UHV) loading arm and could be changed on the beamline, allowing multiple experiments to be performed sequentially without compromising the vacuum. Film growth was achieved using six thermal effusion cells and an electron-beam evaporator at temperatures between 10 and 1200 K. Details of this instrument can be found in Dura and LaRock.[29] For the experiment, only the MBE's vacuum and hydrogen-loading capabilities were applied; however, the investigated Fe/V thin film samples were likely prepared elsewhere by sputtering.[30] Although Dura and LaRock[29] discuss the capability to perform in situ measurements, and the instrument is known to have this capability, no works have been reported using it for performing in situ PNR.

The first PNR studies on films grown directly at a neutron beamline are consequently attributed to Nawrath et al. and Fritzsche et al.:[31,32] at the Helmholtz-Zentrum Berlin (HZB) Fe(001) films with a thickness of up to 20 Å were prepared on V(001) single crystals and investigated in situ using the neutron reflectometer V6. Although these early pioneering experiments were hampered by the available neutron flux, signals could clearly be resolved for layers as thin as 6 Å with data acquisition times of typically 12 h.

Due to the limited neutron flux at the sample position during these early experiments, it was a common belief that PNR measurements of in situ grown films is too time consuming to be compatible with the established proposal-driven scheduling system. Consequently, further development of in situ PNR was largely abandoned. Also, an in situ thin film deposition system, planned for the Spallation Neutron Source (SNS) magnetism reflectometer MAGREF, was never realized.[33]

However, at the Jülich Centre for Neutron Science (JCNS) at the Heinz Maier-Leibnitz Zentrum (MLZ) in Garching, Germany, an MBE growth chamber exists with a vacuum suitcase attachment, allowing samples to be transported to the neutron reflectometer MARIA and measured without breaking the vacuum.[34]

The approach, in principle, allows an in-situ-like growth, in which layers can be sequentially deposited. However, the sample transport over long distances and through radiation protection facilities slows down the measurement sequence and bears the risk of sample contamination. As radiation protection is also a concern, the reverse process of transferring the sample from the beamline back to the growth chamber for resuming sample growth has not been realized.[35,36] Ultimately, an optimized in situ PNR experiment would allow measurements continuously during deposition or in short breaks in-between deposition runs without any change of sample position or beam alignment, (quasi) in operando. To realize these, real-time measurements will require a very high data acquisition rate, achievable by either a high-brilliance neutron source or a support instrumentation with a high signal-to-noise ratio. The massively increased brilliance of the future European Spallation Source (ESS) in combination with novel instrument and improved neutron optical concepts[37–39] will soon allow for even (quasi) in operando experiments, where only an interruption in sample growth of a few seconds is required for the PNR analysis. As an important note, in the proposed scenarios, the growth and measurement temperatures are similar; however, for some systems, such as oxides, which tend to have a high growth temperature and low measurement temperature, in operando measurements will not be possible. Nevertheless, the ability to prepare samples without breaking the vacuum, realigning, and the preparing of sequential layer growth are still beneficial and available with the in situ setup.

Anticipating these upcoming novel neutron sources, the development of a flagship thin film deposition system for PNR was undertaken by the Technical University Munich (TUM), the University of Augsburg (UA), and the Max-Planck Institut (MPI) Stuttgart. The developed system allows for the first time important aspects of material, size limitations, vibrational influences, and geometrical restrictions to be explored and opens up new technological capabilities for in situ PNR. With a design that allows the sample to remain aligned in the neutron beam for alternating layer deposition and measurement processes, it also closes the gap to perform fully in operando thin film growth experiments with PNR analysis.

This new instrument has been demonstrated in the exploration of magnetism in ultrathin Fe layers (Section 3.2) and proximity-induced magnetism in ferromagnetic/nonmagnetic bilayers (Section 3.3).[40,41] In situ PNR was also applied to novel approaches for reconstructing the phase information.[42]

2. Recent Experimental Developments

The general design concept of the most recent deposition system follows a layout that was optimized for use on the reflectometer and evanescent wave small angle neutron spectrometer (REFSANS), operated by the Helmholtz-Zentrum Geesthacht at the MLZ.[43–45] There, the initial stages of the development of the in situ PNR capabilities took place. However, the deposition system is now mainly applied on the AMOR beamline[46] at the Paul Scherrer Institut (PSI), for which it is being developed further and where it is typically operated for scientific use. The unique feature of AMOR is that most components are mounted on an optical bench, which results in a high degree of flexibility for the installation of optical components and sample environments. In particular, the prototype of the focusing Selene neutron optical concept[38,39,47] provides (in situ) PNR data with sufficient statistics in a few minutes of data accumulation time per spin direction. This complies ideally with the requirements for in situ PNR.

2.1. In Situ Thin Film Deposition System

The thin film deposition system incorporated initially only the components necessary to meet basic requirements: 1) a vacuum with $p_{base} \approx 1 \times 10^{-6}$ mbar, generated by a turbo molecular pump; 2) a deposition system, consisting of sputter gas supply and three sputter deposition sources with 2-inch diameter targets that can be rotated above the sample position for keeping the sample aligned in the neutron beam while changing from one deposition material to the other; 3) a magnetic field environment, consisting of guiding fields and a pair of Helmholtz coils for magnetizing the sample (30 mT); and 4) an in and ex vacuum slit system for defining the neutron beam.[48] With this, a proof of concept confirming the feasibility of in situ PNR was demonstrated, in which a Ni/Cr bilayer with nominal thicknesses of 40 nm Ni and 53 nm Cr on a Si substrate was grown step by step in the neutron beam (**Figure 2**).

Although the basic in situ PNR setup proved to be well suited for room temperature investigations of magnetic thin films, many scientifically interesting magnetic systems, such as oxides like Pb(Zr,Ti)O, MgO, and BaTiO,[49–52] additionally required improved vacuum capabilities and elevated temperatures of up to 1000 K for realizing epitaxial thin film growth. However, also temperature ranges significantly below room temperature for the investigation of their magnetic properties[53,54] are needed. In addition, the application of precisely adjustable, high magnetic fields is required if complex magnetic structures are to be grown and investigated in situ by PNR.[55] Responding to these challenges, the design was improved, including a lower base pressure ($p_{base} < 5 \times 10^{-9}$ mbar), sample heating and cooling stage (10–1000 K), and magnetic field capabilities at the sample position (up to 300 mT). The sputtering system was also redesigned to improve the parameter control. This provides researchers with a highly versatile in situ deposition system,[56] as shown in **Figure 3**. Furthermore, the development of a new control software allows the deposition process to be fully scripted and integrated with the beamline control into an automated measurement and deposition sequence.
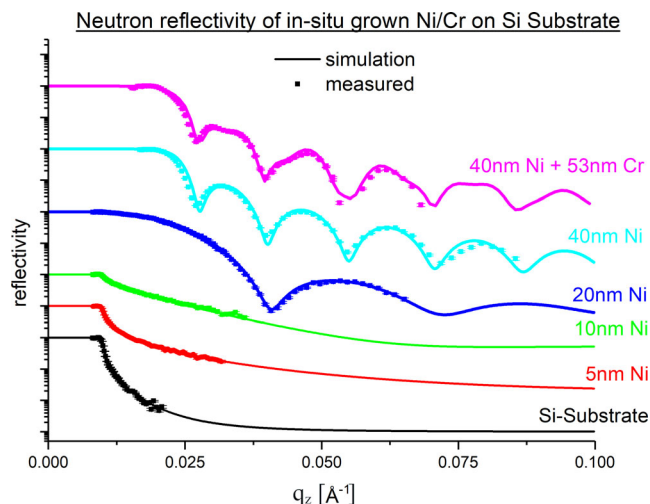

Figure 2. Neutron reflectivity data as measured during the first proof-of-principle experiments, performed using the in situ sputter deposition chamber on REFSANS at the MLZ. The figure shows the measured reflected intensities (points) as a function of the perpendicular momentum transfer q_z, obtained during the step-by-step growth of a Ni/Cr bilayer with nominal thicknesses of 40 nm Ni and 53 nm Cr on a Si substrate as well as the simulated reflectivity curves for each of the growth steps (solid lines). In these measurements the characteristic penetration depth of neutrons causes the critical momentum transfer q_c to be defined by the underlying substrate until a Ni layer thickness of 20 nm is reached.
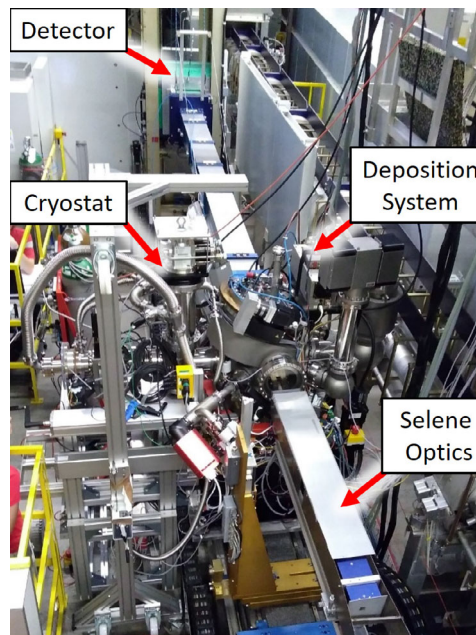

Figure 3. Sputter deposition system and Selene optics, integrated into the AMOR beamline. Photo taken before the recent SINQ upgrade: The blue Selene guide elements in front of the sputtering chamber focus the neutron beam onto the sample, located in the center of the in situ deposition system. Sample cooling and heating are realized by the attached cryostat setup. The scattered neutrons are detected by a 2D detector (turquoise box), located after a flight tube made from aluminum. The neutrons enter and leave the vacuum chamber through fused silica (SiO_2) glass windows.

2.2. Focusing Neutron Optics

For in situ PNR the prototype of the focusing Selene neutron optical concept available on the AMOR beamline at the Swiss spallation neutron source (SINQ), PSI,[38,39,47] was used, offering a high-intensity angular and energy-dispersive data acquisition scheme. This measurement scheme combines traditional angular and energy-dispersive measurement modes into one high-intensity mode by measuring $\alpha_f (= \alpha_i)$ and λ simultaneously, using a pair of Montel mirrors to focus a broad-wavelength-band neutron beam onto the sample (**Figure 4**). In the Selene mode the complete beam is convergent and the sample is in the focal point. Therefore, no further beam-shaping elements are needed. For in situ PNR, the full beam divergence of 1.6° from AMOR is used to illuminate the sample with a neutron wavelength band of 4–10 Å, increasing the effective neutron intensity by a factor of 30 when compared to the conventional collimated PNR operation mode of AMOR. This allows data accumulation with sufficient statistics in a few minutes to be accomplished.

In the Selene mode, the scattering angle 2θ and its resolution Δ2θ depend on the sample–detector distance, the detector position, and its spatial resolution. The neutrons are detected using the time of flight (ToF) from the upline chopper. The resulting 3D data array (γ and z position on the detector and time t) is integrated along the normal to the scattering plane and converted to an $I(\lambda, \theta)$ map. After normalizing by the wavelength-dependent intensities in the incident beam, one obtains the reflectivity $R(\lambda, \theta)$, which in this representation corresponds to a reflectivity curve measured in ToF mode for each θ, and—vice versa—for each λ to a reflectivity curve obtained in angular-dispersive mode. By transforming the data in $R(\mathbf{q})$, where $\mathbf{q}$ is the momentum transfer vector, the data can be collated, resulting in the standard 1D reflectivity curve.

This combination of both measurement schemes reduces the counting time for specular reflectometry by at least one order of magnitude compared to standard collimated measurements and makes AMOR the beamline of choice for in situ PNR.

3. Recent Applications of In Situ Neutron Reflectometry

The technique of in situ PNR has been applied to several scientific questions at hand. In the following, the most recent studies, all performed using the deposition system developed at TUM and UA, will be briefly summarized.

3.1. In Situ Thin Film Growth for ³He Spin Filter Development

The in situ thin film deposition system found its first scientific use in the context of ³He neutron spin filter (NSF) development[57] on REFSANS.

In this work,[41] the research team prepared sequential films of Cu (20 nm) and then Fe (1 nm), grown in situ on the neutron beamline. Between these depositions, the sample was not realigned. The deposition configuration is shown in **Figure 5**, with the magnetostatic cavity[58] containing the NSF. In this study it was critical that the sample was not extracted from vacuum, as this would have resulted in the oxidation of the Cu and ultrathin Fe layers.

3.2. Epitaxial Thin Film Growth of Fe on Cu(001)

In the second study, the evolution of structural and magnetic properties of a stepwise in situ grown epitaxial Fe layer was investigated. The sample was kept aligned in the neutron beam and maintained in vacuum at all times as it is grown step by step to its final thickness. Such results are particularly valuable as variations in growth between different samples—even if grown at a similar time using the same deposition chamber—can result in significant changes in material properties when working on nanoscale structures. On a single sample, the progressive evolution of the microstructure and magnetic properties of a sputter-deposited Fe thin film on a Cu/Si(001) substrate was followed using in situ PNR.[59]
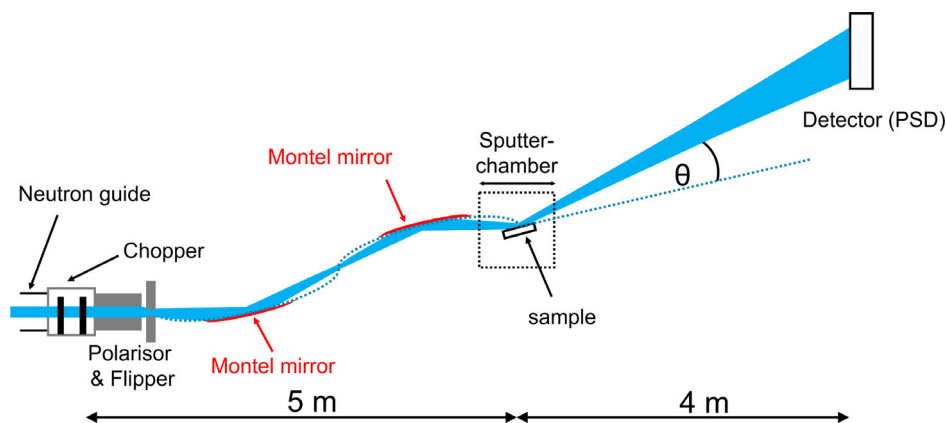

Figure 4. Schematic of the Selene neutron optical concept, shown in combination with the position of the sputter deposition chamber. Divergent, polarized neutron pulses, formed by a chopper system, illuminate a pair of Montel mirrors. These focus the neutron beam with a broad wavelength band of typically 4 Å < λ < 10 Å onto the thin film sample, which reflects the neutrons according to its structural and magnetic properties. The arrival time and position of the reflected neutrons are recorded by an area detector. Because only the useful neutrons are transported by the Selene mirrors, the neutron background is low and no further beam-shaping devices are required.
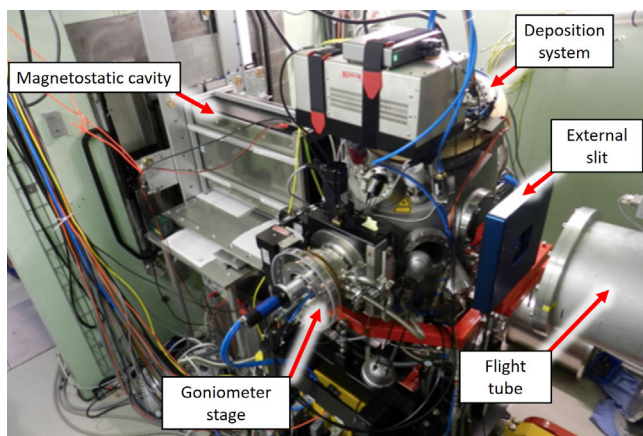
Figure 5. Sputter deposition system, integrated into the REFSANS beamline. A magnetostatic cavity for NSFs is installed between the neutron optics (hidden from view behind the green wall to the left of the photograph) and the in situ deposition system. Details of the goniometer stage with encoder and details of the external slit system are visible, which is located before the entrance window of the evacuated flight tube.

The Fe deposition process was periodically interrupted for the duration of the PNR measurements. Typically, the in situ PNR data acquisition time was 15 min per spin direction, allowing 28 deposition steps to be investigated within less than 1 day of beamtime (**Figure 6**). In each deposition step i the volume of approximately one monolayer of Fe was deposited. From PNR, the number density n_i^{Fe}, thickness d_i^{Fe}, interfacial roughness σ_i^{Fe}, and magnetization M_i^{Fe} of the Fe layer were extracted quantitatively as a function of the deposited amount of material by a fitting process. **Figure 7** shows these accessible microstructural and magnetic parameters and their evolution.

Although the in situ PNR study confirmed most of the known thickness-dependent magnetic properties of Fe layers, the sputter-deposited Fe films were found to exhibit some unique features that were not observed for Fe thin films grown by other techniques. These include indications for a more than 10% larger magnetization in the early nucleation phase of Fe than previously reported in the literature and room temperature magnetism in the thickness regime of 5–11 monolayers of Fe.

Although the understanding of the evolution of Fe films during their growth by sputter deposition is clearly interesting in itself, the studies also demonstrate the potential of in situ PNR for the analysis of magnetic properties on the atomic scale. The fact that even in a widely studied system such as the investigated epitaxial Fe layer new aspects were identified demonstrates that in situ PNR can clearly provide valuable complementary information to photon- and electron-based techniques.

3.3. Dzyaloshinksii–Moriya Interaction at the Pd/Fe Interface

In situ studies are also of particular importance when layer systems are investigated which reveal proximity effects such as induced magnetism. Of these, Pd with its high magnetic
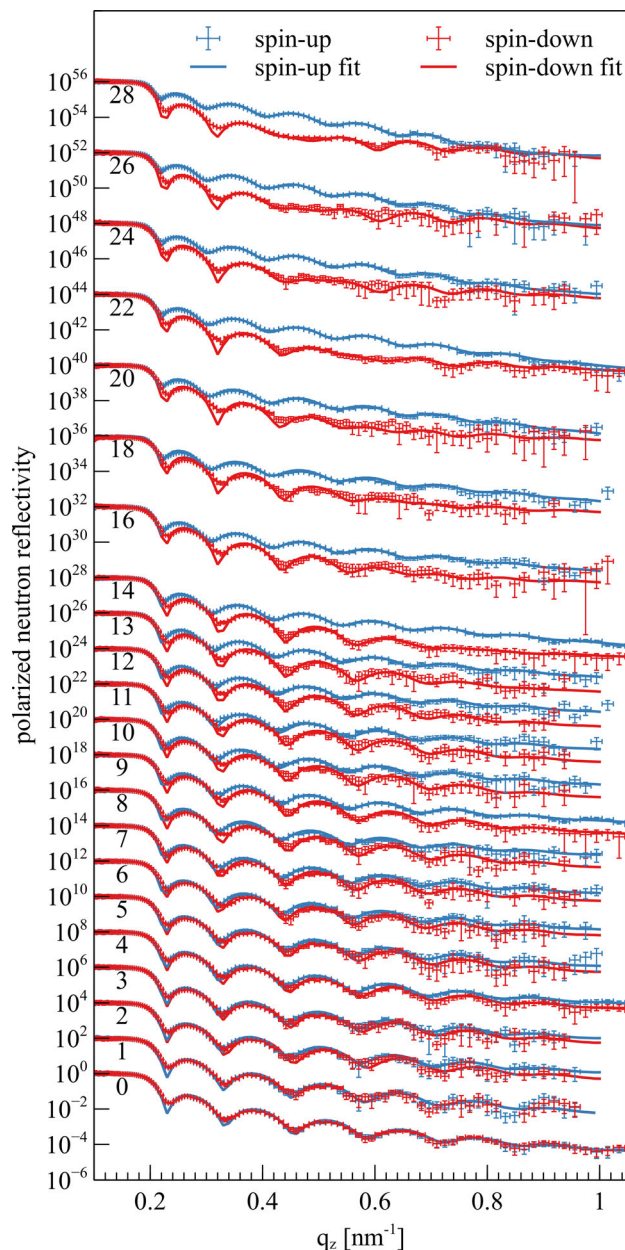

Figure 6. Neutron reflectivity versus the perpendicular momentum transfer q_z of an epitaxially in situ grown Fe layer on Cu/Si(001). The data were obtained with typical PNR acquisition times of $\approx$15 min per spin direction and with each deposition step requiring $\approx$5 min between the PNR measurements. The data are overlaid with fitted reflectivity curves. For reasons of clarity, each pair is vertically shifted by two orders of magnitude, with the number below the regime of total reflection denoting the deposition step i.

susceptibility is the prototypical material. Especially Fe/Pd-based thin films show strong induced magnetism in the Pd, which has been widely studied experimentally[60–67] and theoretically.[65–70] Induced magnetization up to 2 nm from the Fe/Pd interface into the Pd has been observed,[60] with typical values of $0.3 - 0.4\,\mu_B/\text{atom}^{Pd}$ at the interface.[63,65,70]
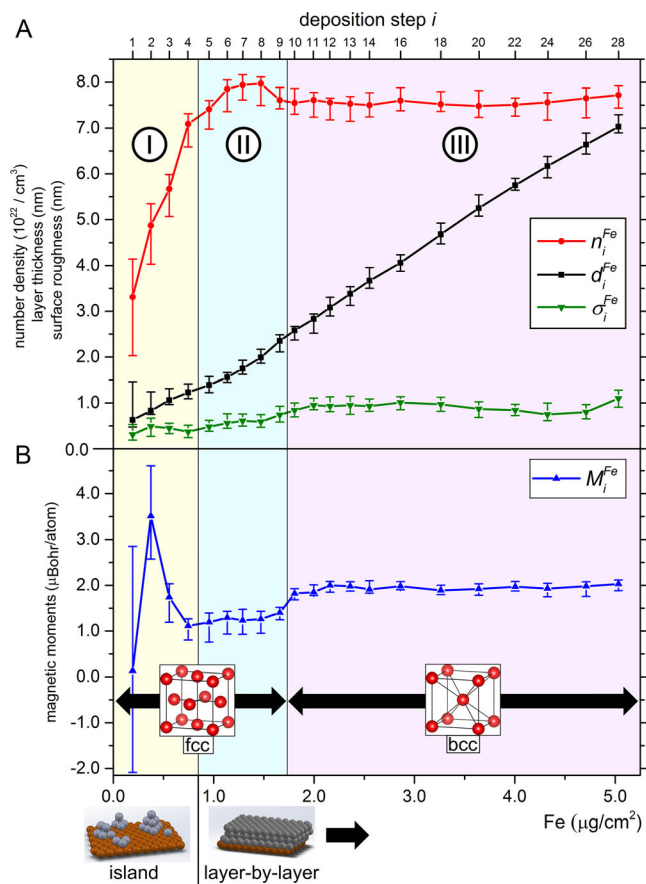
Figure 7. The fit parameters of the epitaxially grown Fe layer as a function of deposition step i. Three main regimes (I–III) with different characteristic behaviors for the number density n_i^{Fe}, thickness d_i^{Fe}, interfacial roughness σ_i^{Fe}, and magnetization M_i^{Fe} can be identified. Shown are also the concluded growth modes (island/layer-by-layer) and crystalline structures (fcc/bcc). Reproduced with permission.[59] Copyright 2017, American Physical Society.

Figure 8. Magnetization profiles of an in situ grown Pd/Fe/Pd trilayer as a function of deposition step $i = 2$–19 of the covering Pd layer, and distance from the center of the Fe layer, obtained from in situ PNR ($i = 1$ denotes the deposition step of the intial Pd layer, $i = A$ is the deposition step, in which the Fe layer was grown). For reasons of clarity, dashed lines show interpolated curves. They are displayed vertically shifted by $1 \mu_B$ atom^{-1}. The regions of induced magnetization in the Pd—denoted as Pd−4, Pd−3, Pd−2, Pd−1 (Pd seed layer) and Pd+1, Pd+2, Pd+3 and Pd+4 (Pd capping layer)—extend up to 0.92 nm to either side of the Fe layer, with the remaining Pd being regarded as nonmagnetic. Although in the initial stages of Pd capping layer growth a strong asymmetry of the magnetization of Pd−1 and Pd+1 is observed, the asymmetry vanishes as the structural symmetry of the Pd/Fe/Pd trilayer is restored. This is accompanied by a slight reduction in the magnetization of the Fe layer.

The evolution of proximity-induced magnetism in Pd(t) ($0 < t < 11$ nm) was followed by in situ PNR as it was deposited on a Fe (0.4 nm)/Pd (11 nm)/Si (substrate) underlayer. Deposition was performed over 18 steps, providing a monolayer-scale understanding of the magnetic proximity effect. This is particularly crucial since this effect is mediated by the exchange interactions, which tend to be extremely short-range, decaying exponentially from the interface. In this case, the in situ PNR data acquisition times were 35 min for each spin direction.

Depth profiles of the local region around the Fe layer are shown in **Figure 8**. Without a Pd capping layer, identified as step A, there is clear long-range proximity-induced magnetism in the Pd underlayer, up to 1.2 nm away from the interface. However, approaching the interface, the magnetism in Pd is abruptly reduced to $0.12 \mu_B$/atom^{Pd}, whereas the Fe magnetization is determined to be $1.6 \mu_B$/atom^{Fe}. Subsequent deposition of the Pd capping layer (steps 2–18) initially further promotes an asymmetric magnetic structure, with the Pd capping layer having larger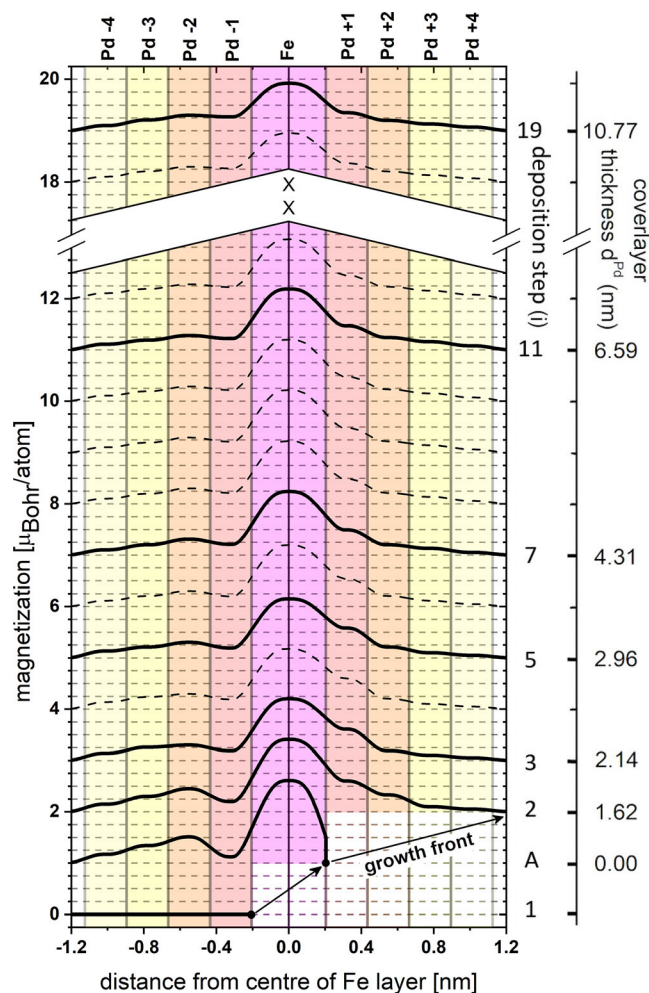 magnetization compared to the underlayer. Upon further increasing the Pd thickness, the Pd layers symmetrize and the Fe moment is reduced.

These observations indicate the presence of proximity-induced magnetism, which extends into the Pd up to > 1 nm on both sides of the Pd/Fe interface and of a Dzyaloshinskii–Moriya interaction directly at the Pd/Fe interface. In particular, it was found that the dominance of either effect and the magnetization of the Pd and Fe layers can experimentally be influenced by restoring the structural and electronic symmetry as Pd is deposited onto the Fe layer.

3.4. Phase Reconstruction

The phase information of a samples's reflection uniquely determines the scattering length density (i.e., the scattering potential) of the sample. Accessing the phase information, however, is impossible with a single PNR experiment. Nevertheless, with in situ PNR this information can be retrieved by means of reference layers[71] at the sample's surface. The thickness of the top layer gradually increases with each deposition step and each additional PNR measurement constrains the feasible phase. After three iterations the reflection is defined unambigiously.

In situ PNR is particularly well suited for this approach because the top reference layer can be varied by increasing its thickness, without the underlying sample being altered by oxidation or contamination of residual molecules by ambient air.

The reference layer method can be applied as long as the buried unknown part is not influenced by varying the top layer as deposition continues. Also, only nonabsorbing materials for the reference layer can be used with this approach.[72] By solving the Gelfand–Levitan–Marchenko integral equation, the scattering potential is reconstructed using the reflectivity and the phase information, assuming no bound states being present in the system.[73]

As a proof of concept, the in situ PNR data of Kreuzpaintner et al.[59] (Figure 6), which were evaluated using a traditional fitting method, were reevaluated for reconstructing the phase information. The monolayers of Fe were used as reference layers and the shape of the references were determined by traditional fitting. In total, 40 PNR measurements were used to constrain the phase information of the Cu/Si(substrate) buried sample. Because the reflection below the critical edge cannot be determined with this approach, the phase information is computed by a model-free algorithm for $q \leq 0.23\,\text{nm}^{-1}$; see Book and Kienzle.[74]

Figure 9 shows the reconstructed reflection and the inverted scattering potential of the Cu seed layer and of a mathematical model with an ideal 43.3 nm thick Cu layer on a Si substrate. Note that the reconstructed reflection does not perfectly match the theoretical model, in particular at the dips and tips of the phase. The discrepancy can be explained by the fact that the data are degraded by resolution effects, whereas the theoretical curve was simulated without taking any resolution effects into account. Also, the oscillations in the reconstructed potential are not necessarily a physical phenomenon, but originate from the limitation in q. This effect is analogous to a truncated Fourier transform, which by principle cannot recover the original data but creates artificial oscillations.

The reconstructed scattering potential is uniquely determined as well as the physical parameters; e.g., the average density of the Cu layer amounts to $(8.86 \pm 0.11)\,\text{g}\,\text{cm}^{-3}$ and its thickness is $\approx 44.6\,\text{nm}$. For comparison, the density and thickness obtained from a traditional fit are $8.82\,\text{g}\,\text{cm}^{-3}$ and 45.1 nm, respectively. As such in situ PNR marks a highly promising approach for finding a universal, standardized experimental procedure, which may even routinely allow a phase retrieval in neutron reflectometry experiments to be performed during data collection.
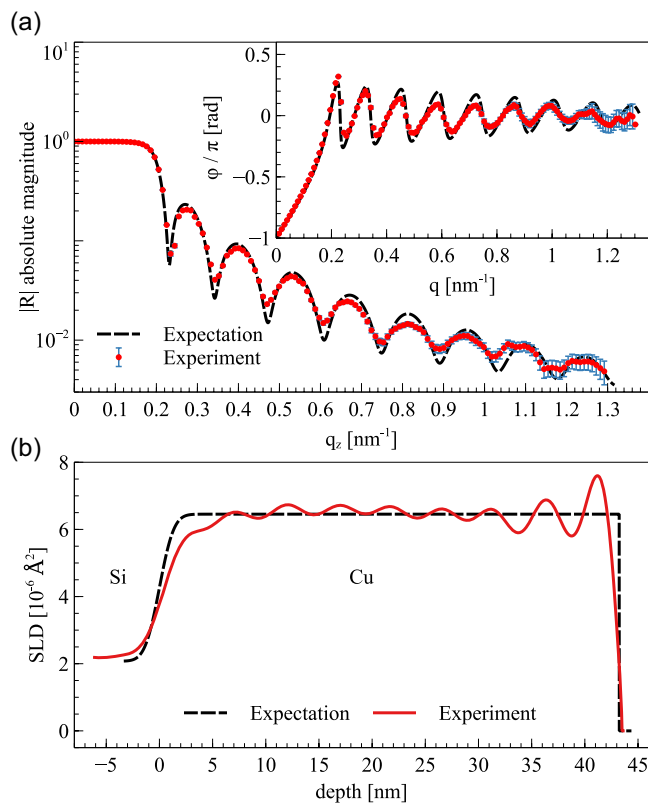

Figure 9. a) The reconstructed reflection $R = |R|e^{i\varphi}$ of the Cu/Si$_{\text{substrate}}$ sample, using the reflectivity data shown in Figure 6. The inset shows the phase information of the reflection. b) Scattering length density of the reconstructed sample, using the reflection shown in the top graph. The depth at 0 nm refers to the Cu/Si interface. "Expectation" represents the reflection and SLD as obtained from traditional fitting.

4. Conclusion

From the pioneering experiments dating back to the 1990s and early 2000s, during the last decade the most significant progress in the field of in situ PNR took place.

In particular, within the collaborative research center TRR 80 project "Neutron Reflectometry on Magnetic Layers," the technique of polarized neutron reflectometry for the investigation of magnetic thin film samples could successfully be combined with in situ ultrahigh-vacuum thin film growth capabilities.[48] The technological solution developed is the current flagship of in situ thin film growth environments for neutron scattering. It allows highly complex heterostructures to be grown and analyzed. Here, the aspect of keeping the sample aligned in the neutron beam at all stages of thin film growth and measurement is the unique feature. If used in combination with the focusing Selene neutron optical concept available on the neutron reflectometer AMOR at PSI, magnetic thin films and heterostructures can be deposited and analyzed by in situ PNR with data acquisition times of only a few minutes, in particular after the current upgrade of SINQ.

The feasibility of characterizing the evolution of magnetic properties in situ by PNR on the atomic scale and even when

only a single atomic layer of Fe or Pd is added to a thin film structure has been demonstrated.[40,59] The developed in situ PNR capabilities have been applied to follow the progressive evolution of the microstructure and magnetic properties of epitaxial Fe on Cu(001)/Si(001). Known features were reproduced and novel aspects identified, which extend our knowledge on the behavior of ultrathin Fe films.[59] Furthermore, recent results on the magnetic proximity effect in Pd/Fe heterostructures were discussed in Section 3.3.

These capabilities are essential for future in situ PNR studies. Here, we present two examples. Of particular interest are currently FeRh/BFO multilayers. These can be grown at 500 °C[75] and therefore within the temperature range of the available cryostat/furnace solution of the in situ growth chamber. Here, the focus lies on interfacial strain engineering and the control of the metamagnetic transition temperature of FeRh. Another research topic is to study the onset and stabilization of room temperature skyrmions in Gd/Fe multilayer thin films[76–78] with a focus on developing an understanding of the mechanisms responsible for the stabilization of nontrivial topology. For this purpose, the magnetic spin texture can be analyzed using in situ PNR.

A typical Lorentz transmission electron microscope (LTEM) image revealing a stripe domain state of a Gd/Fe multilayer film in zero field is shown in **Figure 10**a. The observed stripe domain pattern exhibits domain walls, partially with and without chirality with an underlying periodicity of ≈100 nm. A corresponding small-angle neutron scattering (SANS) pattern revealing the Fourier transform of the ≈100 nm wide stripes is displayed in Figure 10b. By adding Ir layers to the Fe/Gd multilayer structure, various metastable spin objects such as Bloch skyrmions, magnetic bubbles, and antiskyrmions can be created.[79] In this regard, in future studies, the evolution of spin textures as function of film thickness—including Dzyaloshinskii–Moriya interaction—can be investigated using in situ and ex situ neutron scattering[80] techniques such as PNR, SANS, and grazing incidence SANS (GISANS), which is sensitive to the lateral periodicity of skyrmion lattices.

In this context, it is specifically noted that in situ thin film growth is not limited to reflecting geometries, but can be applied to in principle an abundance of other scattering techniques. Of these (polarized) SANS and GISANS are fully complementary for studying the transverse and lateral thin film sample structures and magnetic properties within thin layers as they are grown. In addition, in situ thin film growth can be combined with further complementary techniques, such as positron-based angular correlation of annihilation (ACAR). In this case, positrons can be guided freely in electric fields, which allows a vacuum chamber design to be realized in which the structural and magnetic properties of an in situ grown and evolving thin magnetic film can be followed by PNR while the Fermi-surfaces of a sample's electronic structure is traced simultaneously by ACAR.[81,82]

With respect to data acquisition times of in situ PNR on AMOR and upcoming neutron reflectometers, such as ESTIA at the ESS, the development of a highly automated dedicated fitting software for simultaneous fitting of in situ PNR data, obtained from the very same sample but at different stages of growth, is required. Here the aspect of a significantly faster data evaluation during the course of the experiment is in focus. At present, it is not expected that a full automation of the fitting process can be achieved, but the large amount of a priori knowledge obtained by following the sample with PNR throughout its growth provides certain boundary conditions that allow at least a higher degree of automation to be reached.

The future prospectives of in situ PNR are therefore tantalizing, with this technique allowing investigations of materials during their critical ordering phase. Further improvements to neutron sources and complementary neutron instrumentation and management make these prospects even brighter, potentially including (quasi) in operando real-time measurements during thin film growth.

Figure 10. Magnetic stripe pattern of a [Gd(0.41 nm)/Fe(0.34 nm)] × 80 multilayer imaged by an underfocused LTEM at zero magnetic field and room temperature. b) SANS pattern collected within the ordered stripes state displayed in (a).

Conflict of Interest

The authors declare no conflict of interest.

Keywords

deposition systems, in situ growth, polarized neutron scattering, thin film magnetism
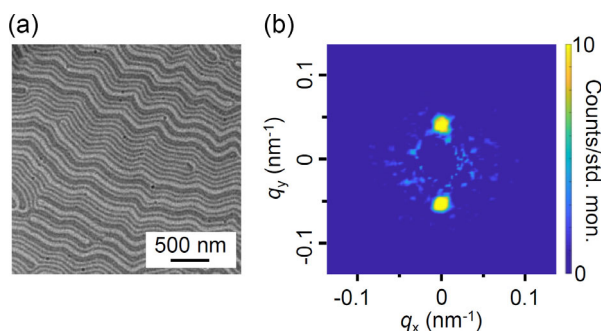
[1] Y. F. Nie, Y. Zhu, C. H. Lee, L. F. Kourkoutis, J. A. Mundy, J. Junquera, P. Ghosez, D. J. Baek, S. Sung, X. X. Xi, K. M. Shen, D. A. Muller, D. G. Schlom, *Nat. Commun.* **2014**, *5*, 4530.

[2] S. Middey, J. Chakhalian, P. Mahadevan, J. Freeland, A. Millis, D. Sarma, *Annu. Rev. Mater. Res.* **2016**, *46*, 305.

[3] M. Gibert, M. Viret, A. Torres-Pardo, C. Piamonteze, P. Zubko, N. Jaouen, J. M. Tonnerre, A. Mougin, J. Fowlie, S. Catalano, A. Gloter, O. Stéphan, J. M. Triscone, *Nano Lett.* **2015**, *15*, 7355.

[4] H. Boschker, J. Mannhart, *Annu. Rev. Condens. Matter Phys.* **2017**, *8*, 145.

[5] H. Zabel, *Appl. Phys. A*, **1994**, *58*, 159.

[6] J. Penfold, R. K. Thomas, *J. Phys.: Condens. Matter* **1990**, *2*, 1369.

[7] D. Gorkov, B. P. Toperverg, H. Zabel, *Nanomaterials* **2020**, *10*, 851.

[8] C. F. Majkrzak, G. P. Felcher, *MRS Bull.* **1990**, *15*, 65.

[9] C. Majkrzak, *Physica B* **1991**, *173*, 75.

[10] H. Zabel, *Physica B* **1994**, *198*, 156.

[11] J. Ankner, G. Felcher, *J. Magn. Magn. Mater.* **1999**, *200*, 741.

[12] G. P. Felcher, *J. Appl. Phys.* **2000**, *87*, 5431.

[13] T. Saerbeck, F. Klose, *Proc. Eng.* **2012**, *36*, 488.

[14] T. J. Smart, J. Mannhart, W. Braun, *J. Laser Appl.* **2021**, *33*, 022008.

[15] U. Rücker, T. Cronert, J. Voigt, J. P. Dabruck, P. E. Doege, J. Ulrich, R. Nabbi, Y. Beßler, M. Butzek, M. Büscher, C. Lange, M. Klaus, T. Gutberlet, T. Brückel, *Eur. Phys. J. Plus* **2016**, *131*, 19.

[16] J. F. Gregg, *Nat. Mater.* **2007**, *6*, 798.

[17] A. Schmehl, V. Vaithyanathan, A. Herrnberger, S. Thiel, C. Richter, M. Liberati, T. Heeg, M. Röckerath, L. Kourkoutis, S. Mühlbauer, P. Böni, D. Muller, Y. Barash, J. Schubert, Y. Idzerda, J. Mannhart, D. Schlom, *Nat. Mater.* **2007**, *6*, 882.

[18] T. Mairoser, J. A. Mundy, A. Melville, D. Hodash, P. Cueva, R. Held, A. Glavic, J. Schubert, D. A. Muller, D. G. Schlom, A. Schmehl, *Nat. Commun.* **2015**, *6*, 7716.

[19] D. A. Gilbert, A. J. Grutter, P. D. Murray, R. V. Chopdekar, A. M. Kane, A. L. Ionin, M. S. Lee, S. R. Spurgeon, B. J. Kirby, B. B. Maranville, A. T. N'Diaye, A. Mehta, E. Arenholz, K. Liu, Y. Takamura, J. A. Borchers, *Phys. Rev. Mater.* **2018**, *2*, 104402.

[20] D. A. Gilbert, J. Olamit, R. K. Dumas, B. J. Kirby, A. J. Grutter, B. B. Maranville, E. Arenholz, J. A. Borchers, K. Liu, *Nat. Commun.* **2016**, *7*, 11050.

[21] A. J. Grutter, D. A. Gilbert, U. S. Alaan, E. Arenholz, B. B. Maranville, J. A. Borchers, Y. Suzuki, K. Liu, B. J. Kirby, *Appl. Phys. Lett.* **2016**, *108*, 082405.

[22] P. D. Murray, D. A. Gilbert, A. J. Grutter, B. J. Kirby, D. Hernández-Maldonado, M. Varela, Z. E. Brubaker, W. L. N. C. Liyanage, R. V. Chopdekar, V. Taufour, R. J. Zieve, J. R. Jeffries, E. Arenholz, Y. Takamura, J. A. Borchers, K. Liu, *ACS Appl. Mater. Interfaces* **2020**, *12*, 4741.

[23] N. F. Berk, C. F. Majkrzak, *Phys. Rev. B* **1995**, *51*, 11296.

[24] M. Yoshimoto, H. Nagata, T. Tsukahara, H. Koinuma, *Jpn. J. Appl. Phys.* **1990**, *29*, L1199.

[25] W. Matz, N. Schell, W. Neumann, J. Bøttiger, J. Chevallier, *Rev. Sci. Instrum.* **2001**, *72*, 3344.

[26] O. M. Magnussen, J. Hotlos, R. J. Nichols, D. M. Kolb, R. J. Behm, *Phys. Rev. Lett.* **1990**, *64*, 2929.

[27] P. Lavalle, C. Gergely, F. J. G. Cuisinier, G. Decher, P. Schaaf, J. C. Voegel, C. Picart, *Macromolecules* **2002**, *35*, 4458.

[28] B. Hjörvarsson, J. A. Dura, P. Isberg, T. Watanabe, T. J. Udovic, G. Andersson, C. F. Majkrzak, *Phys. Rev. Lett.* **1997**, *79*, 901.

[29] J. A. Dura, J. LaRock, *Rev. Sci. Instrum.* **2009**, *80*, 073906.

[30] P. Isberg, B. Hjörvarsson, R. Wäppling, E. Svedberg, L. Hultman, *Vacuum* **1997**, *48*, 483.

[31] T. Nawrath, H. Fritzsche, F. Klose, J. Nowikow, H. Maletta, *Phys. Rev. B* **1999**, *60*, 9525.

[32] H. Fritzsche, Y. T. Liu, J. Hauschild, H. Maletta, *Phys. Rev. B* **2004**, *70*, 214406.

[33] F. Klose, private communication.

[34] A. S. Mohd, S. Pütter, S. Mattauch, A. Koutsioubas, H. Schneider, A. Weber, T. Brückel, *Rev. Sci. Instrum.* **2016**, *87*, 123909.

[35] S. Mattauch, private communication, **2018**.

[36] A. Syed Mohd, private communication, **2021**.

[37] Description of CANDOR, https://ncnr.nist.gov/equipment/msnew/ncnr/candor-description.html (accessed: March 2021).

[38] J. Stahn, U. Filges, T. Panzner, *Eur. Phys. J. Appl. Phys.* **2012**, *58*, 11001.

[39] J. Stahn A. Glavic, *Nucl. Instrum. Methods Phys. Res. A* **2016**, *821*, 44.

[40] S. Mayr, J. Ye, J. Stahn, B. Knoblich, O. Klein, D. A. Gilbert, M. Albrecht, A. Paul, W. Kreuzpaintner, *Phys. Rev. B* **2020**, *101*, 024404.

[41] W. Kreuzpaintner, S. Masalovich, J. F. Moulin, B. Wiedemann, J. Ye, S. Mayr, A. Paul, M. Haese, M. Pomm, P. Böni, *Nucl. Instrum. Methods Phys. Res. A* **2017**, *848*, 144.

[42] A. Book, S. Mayr, J. Stahn, P. Böni, W. Kreuzpaintner, arXiv:2102.10028 [astro-ph, physics:physics, stat] **2021**.

[43] R. Kampmann, M. Haese-Seiller, V. Kudryashov, B. Nickel, C. Daniel, W. Fenzl, A. Schreyer, E. Sackmann, J. Rädler, *Physica B: Condens. Matter*, **2006**, *385–386*, 1161.

[44] R. Kampmann, M. Haese-Seiller, V. Kudryashov, V. Deriglazov, M. Tristl, C. Daniel, B. Toperverg, A. Schreyer, E. Sackmann, *Physica B: Condens. Matter* **2004**, *350*, E763.

[45] J. F. Moulin, M. Haese-Seiller, *JLSRF* **2015**, *1*, A9.

[46] M. Gupta, T. Gutberlet, J. Stahn, P. Keller, D. Clemens, *Pramana* **2004**, *63*, 57.

[47] J. Stahn, T. Panzner, U. Filges, C. Marcelot, P. Böni, *Nucl. Instrum. Methods Phys. Res. A* **2011**, *634*, S12.

[48] A. Schmehl, T. Mairoser, A. Herrnberger, C. Stephanos, S. Meir, B. Förg, B. Wiedemann, P. Böni, J. Mannhart, W. Kreuzpaintner, *Nucl. Instrum. Methods Phys. Res. A* **2018**, *883*, 170.

[49] D. Cáceres, I. Colera, I. Vergara, R. González, E. Román, *Vacuum* **2002**, *67*, 577.

[50] K. Fujimoto, Y. Kobayashi, K. Kubota, *Thin Solid Films* **1989**, *169*, 249.

[51] Y. Kaneko, N. Mikoshiba, T. Yamashita, *Jpn. J. Appl. Phys* **1991**, *30*, 1091.

[52] P. M. Leufke, R. Kruk, D. Wang, C. Kübel, H. Hahn, *AIP Adv.* **2012**, *2*, 032184.

[53] S. Mühlbauer, P. Böni, R. Georgii, A. Schmehl, D. Schlom, J. Mannhart, *J. Phys.: Condens. Matter* **2008**, *20*, 104230.

[54] F. Ott, *J. Phys.: Condens. Matter* **2008**, *20*, 264009.

[55] J. C. Gallagher, K. Y. Meng, J. T. Brangham, H. L. Wang, B. D. Esser, D. W. McComb, F. Y. Yang, *Phys. Rev. Lett.* **2017**, *118*, 027201.

[56] J. Ye, A. Book, S. Mayr, H. Gabold, F. Meng, H. Schäfferer, R. Need, D. Gilbert, T. Saerbeck, J. Stahn, P. Böni, W. Kreuzpaintner, *Nucl. Instrum. Methods Phys. Res. A* **2020**, *964*, 163710.

[57] M. Batz, S. Baeßler, W. Heil, E. W. Otten, D. Rudersdorf, J. Schmiedeskamp, Y. Sobolev, M. Wolf, *J. Res. Natl. Inst. Stand. Technol.* **2005**, *110*, 293.

[58] A. Petoukhov, V. Guillard, K. Andersen, E. Bourgeat-Lami, R. Chung, H. Humblot, D. Jullien, E. Lelievre-Berna, T. Soldner, F. Tasset, M. Thomas, *Nucl. Instrum. Methods Phys. Res. A* **2006**, *560*, 480.

[59] W. Kreuzpaintner, B. Wiedemann, J. Stahn, J. F. M. C. Moulin, S. Mayr, T. Mairoser, A. Schmehl, A. Herrnberger, P. Korelis,

M. Haese, J. Ye, M. Pomm, P. Böni, J. Mannhart, *Phys. Rev. Appl.* **2017**, *7*, 054004.

[60] T. P. A. Hase, M. S. Brewer, U. B. Arnalds, M. Ahlberg, V. Kapaklis, M. Björck, L. Bouchenoire, P. Thompson, D. Haskel, Y. Choi, J. Lang, C. Sánchez-Hanke, B. Hjörvarsson, *Phys. Rev. B* **2014**, *90*, 104403.

[61] Z. Celinski, B. Heinrich, J. F. Cochran, W. B. Muir, A. S. Arrott, J. Kirschner, *Phys. Rev. Lett.* **1990**, *65*, 1156.

[62] C. Liu S. D. Bader, *Phys. Rev. B* **1991**, *44*, 2205.

[63] J. Vogel, A. Fontaine, V. Cros, F. Petroff, J. P. Kappler, G. Krill, A. Rogalev, J. Goulon, *J. Magn. Magn. Mater.* **1997**, *165* 96.

[64] J. Childress, R. Kergoat, O. Durand, J. M. George, P. Galtier, J. Miltat, A. Schuhl, *J. Magn. Magn. Mater.* **1994**, *130* 13.

[65] E. E. Fullerton, D. Stoeffler, K. Ounadjela, B. Heinrich, Z. Celinski, J. A. C. Bland, *Phys. Rev. B* **1995**, *51*, 6364.

[66] O. Rader, E. Vescovo, J. Redinger, S. Blügel, C. Carbone, W. Eberhardt, W. Gudat, *Phys.: Rev. Lett.* **1994**, *72*, 2247.

[67] S. K. Lee, J. S. Kim, B. Kim, Y. Cha, W. K. Han, H. G. Min, J. Seo, S. C. Hong, *Phys. Rev. B* **2001**, *65*, 014423.

[68] M. Pärnaste, M. Marcellini, E. Holmström, N. Bock, J. Fransson, O. Eriksson, B. Hjörvarsson, *J. Phys.: Condens. Matter* **2007**, *19*, 246213.

[69] Z. P. Shi, B. M. Klein, *Phys. Rev. B* **1995**, *52*, 12516.

[70] S. Blügel, B. Drittler, R. Zeller, P. H. Dederichs, *Appl. Phys. A* **1989**, *49*, 547.

[71] C. F. Majkrzak, N. F. Berk, U. A. Perez-Salas, *Langmuir* **2003**, *19*, 7796.

[72] C. F. Majkrzak, N. F. Berk, *Phys. Rev. B* **1995**, *52*, 10827.

[73] P. E. Sacks, *Wave Motion*, **1993**, *18*, 21.

[74] A. Book, P. A. Kienzle, *Phys. B Condens. Matter* **2020**, *588*, 412181.

[75] A. Giampietri, G. Drera, I. Pš, E. Magnano, L. Sangaletti, *Appl. Phys. Lett.* **2016**, *109*, 132903.

[76] J. C. T. Lee, J. J. Chess, S. A. Montoya, X. Shi, N. Tamura, S. K. Mishra, P. Fischer, B. J. McMorran, S. K. Sinha, E. E. Fullerton, S. D. Kevan, S. Roy, *Appl. Phys. Lett.* **2016**, *109*, 022402.

[77] S. A. Montoya, S. Couture, J. J. Chess, J. C. T. Lee, N. Kent, D. Henze, S. K. Sinha, M. Y. Im, S. D. Kevan, P. Fischer, B. J. McMorran, V. Lomakin, S. Roy, E. E. Fullerton, *Phys. Rev. B* **2017**, *95*, 024415.

[78] J. Zhang, X. Zhang, H. Chen, Y. Guang, X. Zeng, G. Yu, S. Zhang, Y. Liu, J. Feng, Y. Zhao, Y. Zhou, X. Qiu, X. Han, Y. Peng, X. Zhang, *Appl. Phys. Lett.* **2020**, *116*, 142404.

[79] M. Heigl, S. Koraltan, M. Vaňatka, R. Kraft, C. Abert, C. Vogler, A. Semisalova, P. Che, A. Ullrich, T. Schmidt, J. Hintermayr, D. Grundler, M. Farle, M. Urbánek, D. Suess, M. Albrecht, *Nature Commun.* **2021**, *12*, 2611.

[80] R. D. Desautels, L. DeBeer-Schmitt, S. A. Montoya, J. A. Borchers, S. G. Je, N. Tang, M. Y. Im, M. R. Fitzsimmons, E. E. Fullerton, D. A. Gilbert, *Phys. Rev. Mater.* **2019**, *3*, 104406.

[81] C. Hugenschmidt, private communication, **2017**.

[82] P. Böni, private communication, **2021**.

Wolfgang Kreuzpaintner is a full professor at the Spallation Neutron Source Science Center, appointed by the Institute of High Energy Physics, Chinese Academy of Sciences (CAS). He obtained his Ph.D. degree in physics in 2010 from the University of Hamburg. After a postdoctoral period at the Technical University of Munich, he habilitated himself in the field of in situ polarized neutron reflectometry in 2019. His expertise is with the development of neutron instrumentation, vacuum technology, and thin film growth. His research interests are with novel spintronic materials and multiferroic and magnetic thin film materials with applications in future storage devices.

Manfred Albrecht received his Ph.D. degree in physics from the University of Konstanz (Germany) in 1999 and spent his postdoctoral time at the IBM Almaden Research Center in San Jose (USA). Afterwards he joined again the University of Konstanz heading an Emmy-Noether research group. In 2007, he was appointed Professor for Experimental Physics with the Chemnitz University of Technology (Germany). In 2013, he was appointed Chair of Experimental Physics IV at the University of Augsburg (Germany). His current research activities include magnetic thin films and nanostructures for spintronic applications (e.g., sensorics, THz emitters), as well as thermoelectric thin films.

Jochen Mannhart is Director, Max Planck Institute for Solid State Research, Stuttgart. His research interests focus on quantum devices built from complex electronic materials. The efforts of the teams he was working in resulted in the discovery of bicrystal Josephson junctions and SQUIDs, the enhancement of critical currents of high-T_c superconductors by grain alignment, the first imaging of atoms with subatomic resolution, the fabrication of the first all-oxide FETs, and the discovery that quantum mechanics contradicts thermodynamics. He has received the Gottfried Wilhelm Leibniz-Preis and the Europhysics Prize.
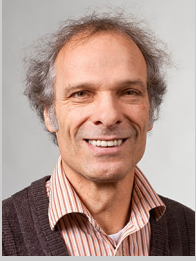
Peter Böni is a retired full professor in the physics department of the Technical University of Munich. He received his Ph.D. degree in physics from ETH Zurich, where he investigated growing ice crystals using dynamic light scattering. Before being appointed Chair of Neutron Scattering at TUM in 2000, he became exposed to neutron scattering at Brookhaven National Laboratory, USA, and at Paul Scherrer Institute, Switzerland. His research focuses on the investigation of magnetic excitations in strongly correlated electron systems using polarized neutrons and in instrumentation for neutron scattering. He received the Europhysics Prize for the discovery of skyrmions in MnSi.